Mass-Selected Ion Mobility Studies of the Isomerization of the Benzene Radical Cation and Binding Energy of the Benzene Dimer Cation. Separation of Isomeric Ions by Dimer Formation

Mark Rusyniak, Yehia Ibrahim, Edreese Alsharaeh, Michael Meot-Ner (Mautner), and M. Samy El-Shall*

Department of Chemistry, Virginia Commonwealth University, Richmond, Virginia 23284-2006

Received: April 1, 2003; In Final Form: June 16, 2003

A mass-selected, ion mobility drift-cell technique has been used to study the isomerization of the benzene radical cation generated by electron impact (EI) ionization. Evidence is presented for the generation of both the benzene and fulvene cations, with a lower limit for the barrier of isomerization E_a(benzene$^{+\bullet}$ → fulvene$^{+\bullet}$) estimated as $E_a > 1.6$ eV. The reduced mobilities of the benzene and fulvene cations are nearly similar, making it difficult to separate the two ions in pure helium. However, because of the large difference in the bonding of the benzene and fulvene cations with neutral benzene, the two isomeric ions are readily separated in the presence of neutral benzene in the drift cell. This suggests that isomer ions with similar mobilities can be separated on the basis of the degree of their associations with their neutral precursor in the drift cell. This separation concept allows us to discover the "hidden isomerization" process responsible for the generation of the fulvene cations via EI ionization of benzene. This also allows us to measure the equilibrium constant for the formation of the benzene dimer cation without interference from the fulvene isomer. The resulting binding energies (17.6 and 17.4 kcal/mol for $(C_6H_6)_2^{+\bullet}$ and $(C_6D_6)_2^{+}$, respectively) are smaller than that reported by Hiraoka and co-workers (*J. Chem. Phys.* **1991**, *95*, 8413) and similar to that measured by Meot-Ner et al. (*J. Am. Chem. Soc*. **1978**, *100*, 5466), both using pulsed high-pressure mass spectrometry. The binding energies of the proton-bound dimers in pyridine and triethylamine systems have been measured as 25.2 ± 1 and 20.9 ± 1 kcal/mol, respectively, and the binding energies of the protonated methanol clusters $H^+(CH_3OH)_n$ with $n = 3-5$ have been measured as 21.0, 14.3, and 11.3 kcal/mol, respectively, in good agreement with literature values. The combination of thermochemical properties with isomer identification provides valuable information on the structure−property relationship of molecular cluster ions. The novel concept of the separation of isomeric ions by dimer formation is expected to be of general application and may help to resolve important outstanding issues in the separation, structure, and chemistry of hydrocarbon radical cations.

I. Introduction

The interaction between a benzene radical cation and neutral benzene is of fundamental interest as a prototype system for studying key interactions between aromatic π systems.[1−8] These interactions play critical roles in diverse areas such as protein structures, base pair stacking in DNA, drug design, crystal packing of aromatic molecules, and the conductivity of organic complexes.[3−8] For a molecular-level understanding of these interactions, the nature of bonding, energetics, and structures of model systems such as benzene cluster ions must be thoroughly investigated.

Despite extensive experimental and theoretical efforts in studying the benzene$^+$/benzene interaction, clear knowledge and a consistent understanding of the binding energy, structure, and isomerization in this system are still limited.[9−19] This view is clearly evident by reviewing the values reported for the binding energy of the dimer cation in the NIST database, which includes a wide range of values from 10 to 21 kcal/mol.[20] Several methods including thermochemical equilibria of the monomer/dimer ions and tunable photoionization of the neutral dimer have been employed in these measurements.[10−19] The binding energy of 17.0 kcal/mol measured by Meot-Ner et al. using high-pressure mass spectrometry (HPMS) was generally considered to be the most reliable value.[11] However, Hiraoka and co-workers using a similar HPMS technique obtained a significantly larger value of 20.6 kcal/mol and suggested that exothermic charge-transfer reactions might result in ring opening of the benzene radical cation in Meot-Ner's experiments.[17] It should be noted that in both HPMS experiments the benzene cation was generated using a sequence of chemical ionization processes within a reaction cell containing a mixture of gases including benzene. Possible contributions from different isomers and side reactions initiated by fragment ions could disturb the true equilibrium between the monomer and dimer cations. However, photoionization experiments of the neutral benzene dimer yield a binding energy of the dimer cation that is significantly lower than both HPMS values.[14,19] The discrepancy in the measured binding energy may suggest that different stable isomers of the dimer cation could have been involved in different measurements. Therefore, it appears that there is a need for new experiments designed to measure the binding energy of a mass-selected and isomer-specific benzene dimer cation. An ideal experiment would allow the injection and thermalization of a well-characterized benzene radical cation into a gas mixture containing a known concentration of benzene held at a controlled

* Corresponding author. E-mail: selshall2@mail1.vcu.edu.

10.1021/jp034850n CCC: $25.00
Published on Web 08/26/2003

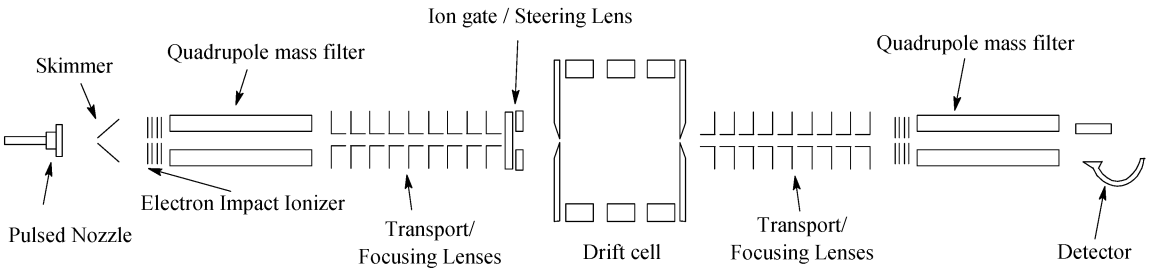

Figure 1. Experimental setup for the mass-selected ion mobility system.

temperature. In addition, the approach to equilibrium between the monomer and dimer radical cations must be directly established.

In the present work, we use a mass-selected drift-cell technique[21−27] to study the dimerization reaction between the isomer-specific benzene radical cation $(C_6H_6)^+$ and neutral benzene as a function of temperature. Using this technique, we will show that electron impact ionization of benzene and exothermic charge-transfer reactions can result in the generation of a mixture containing, in addition to benzene cations, a significant amount of the fulvene cation that corresponds to a neutral precursor with a lower ionization potential than that of the benzene molecule.[20] By separating the fulvene cation, accurate measurements of the enthalpy ($-\Delta H°$) and entropy ($-\Delta S°$) changes of the dimer formation in both the $(C_6H_6)^+$-(C_6H_6) and $(C_6D_6)^+(C_6D_6)$ systems are carried out. The results provide the first measurement of the dimerization equilibrium in a mass-selected and isomer-specific benzene radical cation with neutral benzene. We also extend the equilibrium measurements to two other systems involving proton-bound dimers, namely, $H^+(\text{pyridine})_2$ and H^+ (triethylamine)$_2$. Furthermore, we apply the same method to measure the thermochemistry ($\Delta H°$ and $\Delta S°$) of formation of protonated methanol clusters $H^+(CH_3OH)_n$ with $n = 3-5$. These clusters have been the subject of several previous studies,[28−30] and the current measurements serve as additional checks on our new apparatus over a wide temperature range. These results allow us to establish the mass-selected drift-tube technique as a valuable method for obtaining thermodynamic data on well-defined isomers of molecular cluster ions. The application of this technique to obtain structural information on the benzene cluster cations, $(C_6H_6)_n^+$ with $n = 2-6$, will be presented elsewhere.[31]

II. Experimental Section

A. Instrument. Figure 1 illustrates the experimental setup, which consists of four differentially pumped vacuum chambers. The source chamber is a 12-in. cube evacuated by an unbaffled Varian VHS-6 diffusion pump (3000 L/s in He). This chamber hosts a pulsed valve (general valve no. 9) coupled to a conical nozzle (200-μm diameter) used for the introduction of the vapor sample or the generation of molecular clusters via supersonic adiabatic expansion. During operation, benzene vapor (Aldrich, 99.9% purity) in He or Ar (ultrahigh purity, Spectra Gases 99.99%) at a pressure of 2−5 atm is expanded through the nozzle in pulses of 200−300 μs duration at repetition rates of 50−100 Hz. The average pressure during operation in this chamber is typically $(4-8) \times 10^{-5}$ Torr. The jet is skimmed into a beam by a 3-mm aluminum conical skimmer and passed into the second chamber pumped by an Edward Diffstak 160/700M diffusion pump (1300 L/s in He). The second chamber hosts an electron impact (EI) ionization source coupled to a set of ion lenses and a quadrupole mass spectrometer (Extrel 4000). The quadrupole assembly has a vented shroud for improved pumping, and the chamber is maintained at $(1-5) \times 10^{-6}$ Torr during operation. The emission current in the source is maintained at 1 mA by current regulation at a fixed electron energy ranging from 30 to 100 eV. The resulting ions formed by EI are separated and mass selected by a quadrupole mass filter. The mass filter is typically operated at better than 1 amu mass resolution up to 1000 amu. An exit lens on the quadrupole with 7.5-mm diameter limits the communication between the second and third chambers. The third chamber, which hosts one set of lens stacks, the drift cell, and a second set of ion optics, is pumped by an Edwards Diffstak 250/2000P diffusion pump (3000 L/s in He).

An ion gate located just prior to the drift-cell entrance chops the pulsed ion beam to a narrow 5−50-μs-wide packet, which is then injected into the drift cell. The ions' translational energy is rapidly thermalized through collisions with helium, where the ions drift under the influence of a weak uniform electric field. After traveling across the drift cell, the small fraction of ions that exits is focused into a second quadrupole mass spectrometer. This quadrupole (Extrel-4000 equipped with a mass filter with a 9.5-mm pole diameter) is housed in the fourth chamber, which is pumped by an Edward Diffstak 160/700M diffusion pump (1300 L/s in He) and is typically maintained at $8 \times 10^{-8} - 4 \times 10^{-7}$ Torr. This quadrupole is used to transmit only the ion of interest for measuring the arrival time distribution (ATD). Alternatively, the quadrupole is scanned to determine the dissociation or reaction products that may be formed in the cell. After exiting the quadrupole, ions are detected by an off-axis collision dynode and electron multiplier. The ion gate pulse simultaneously triggers a multichannel scalar scan in order to measure the ATDs of the selected ions exiting the cell.

The drift cell consists of three oxygen-free electrolytic (OFE) copper rings electrically isolated from each other by ceramic spacers on the outside of the cell. The inner diameter and length of the total cell are 8.1 and 8.9 cm, respectively. A series of four resistors, forming a voltage divider network, supply the potentials to the guard rings, which result in a uniform electric field across the cell that can be varied from 1 to 11 V/cm. The end plates are electrically isolated from the guard rings with thin Teflon gaskets. Two sets of end plates are used with orifices of 0.5- and 1-mm diameters, allowing operating pressures of 5−7 and 1−4 Torr of He, respectively. The upper limit of the allowable pressure in the cell is determined by the pumping capacity and the size of the apertures on the cell entrance and exit plates. Using the 0.5-mm apertures, it is possible to maintain a pressure of 10 Torr of He in the cell while maintaining the third chamber pressure at 1×10^{-4} Torr. Two-cartridge resistance heaters inserted in each guard ring can heat the cell to the desired temperature up to 550 K. Temperature controllers (Omega no. CN32S1) are used to maintain constant temperature within ±1°. The temperature of the cell is monitored via K-type thermocouples (two attached to every guard ring and one attached to the exit plate near the orifice).

B. Equilibrium Measurements. Mass-selected $C_6H_6^+$ ions are injected (in 5 −15 μs pulses) into the drift cell containing a known concentration of benzene in a He buffer gas at fixed total pressure and constant temperature. Most of the measurements are carried out with the partial pressure of benzene in the $(1-5) \times 10^{-2}$ Torr range and a total pressure of 2 Torr. The helium carrier gas flows over a temperature-controlled glass bubbler containing liquid benzene, thus forming a saturated vapor mixture of benzene in helium. Flow controllers (MKS no. 1479A) are used to maintain a constant pressure inside the drift cell. The ATDs of injected $C_6H_6^+$ and $(C_6H_6^+)_2$ formed inside the cell are measured as a function of the drift voltage across the cell. The ion intensity ratio $(C_6H_6^+)_2/C_6H_6^+$ is measured from the integrated peak areas of the ATDs as a function of decreasing cell drift field corresponding to increasing reaction time until a constant ratio is obtained. This condition indicates that equilibrium is achieved and that the increase in the effective ion temperature due to the drift field is negligible. The injection energies used in the experiments (10−20 eV, laboratory frame) are slightly above the minimum energies required to introduce the ions into the cell against the He flow. These energies increase by increasing the pressure in the cell. In our experiments at low injection energies, most of the ion thermalization occurs outside the cell entrance by collisions with the helium escaping from the cell entrance orifice. At a cell pressure of 2 Torr, the number of collisions that $C_6H_6^+$ encounters from the helium atoms within a 1-ms residence time inside the cell is about 6×10^4 collisions, which is sufficient to ensure efficient thermalization of the $C_6H_6^+$ ions.

A good test of equilibrium comes from the identical ATDs of the monomer and dimer peaks. If the $C_6H_6^+$ and $(C_6H_6^+)_2$ ions are in equilibrium, then their ATDs must be identical. If the fractional abundances of the monomer and dimer are 1:1, then each of the species spends equal amounts of time being monomer and dimer ions; therefore, their apparent mobilities are equal. If the $C_6H_6^+$ has two peaks corresponding to different isomers, then comparing the $C_6H_6^+$ and $(C_6H_6^+)_2$ ATDs will show which isomer is in equilibrium with the dimer ion $(C_6H_6^+)_2$.

To check further that the equilibrium was achieved, we varied the residence time of the ions in the cell (at 353 K, containing 5.5×10^{-2} Torr C_6H_6 in 2.0 Torr He) between 0.7 and 1.5 ms by varying the electric field across the cell. Above residence times of 1 ms,the equilibrium constant was invariant, supporting equilibrium. All of the equilibrium experiments at different temperatures were conducted at correspondingly low drift fields and long residence times. We also checked equilibrium by verifying that the equilibrium constant was invariant at different helium pressures between 1 and 2.5 Torr and benzene partial pressures between $(1-5) \times 10^{-2}$ Torr. In the equilibrium measurements with a partial pressure of benzene in the range of $(1-5) \times 10^{-2}$ Torr, the number of $C_6H_6^+/C_6H_6$ collisions leading to equilibrium within a 1 ms residence time is estimated to be 300−1500 collisions. Collisional dissociation of the dimer ions after exiting the drift cell or in the second quadrupole was avoided by using a very low acceleration field between the cell and the quadrupole and by maintaining a low pressure in the quadrupole chamber (8×10^{-8} to 4×10^{-7} Torr). Also, the experimental conditions (neutral concentration and temperature) were adjusted to keep the dimer/monomer ion ratio within the 0.1−5 range.

C Mobility Measurements. The mobility K of an ion is defined as[32]

$$K = \frac{\vec{v}_d}{\vec{E}} \tag{1}$$

where $\vec{v}_d$ is the drift velocity and $\vec{E}$ is the field across the drift region. The reduced mobility K_0 (scaled to the number density at standard temperature and pressure STP) is given by

$$K_0 = \frac{P \cdot 273.15}{760 \cdot T} K \tag{2}$$

where P is the pressure in Torr and T is the temperature in Kelvin. Equations 1 and 2 can be combined and rearranged to give

$$t_d = \left(\frac{l^2 \cdot 273.15}{T \cdot 760} \frac{1}{K_0} \right) \frac{P}{V} + t_0 \tag{3}$$

where l is the drift length, t_d is the measured mean arrival time of the drifting ion packet taken from the center of the arrival time distribution (ATD) peak, t_0 is the time the ion spends outside the drift cell before reaching the detector, and V is the voltage across the drift cell. All of the mobility measurements were carried out in the low-field limit where the ion's drift velocity is small compared to the thermal velocity and the ion mobility is independent of the field strength. ($E/N < 5.0$; E is the electric field intensity, N is the gas number density, and E/N is expressed in units of townsend (Td), where 1 Td = 10^{-17} V · cm^2.[32])

Mobility measurements are made by injecting a narrow pulse (5 to 50 μs) of ions into the drift cell. As the ions are injected into the drift cell, the injection energy is dissipated in collisions with the helium buffer gas. Upon exiting the cell, the ions are collected and refocused into the second quadrupole for analysis and detection. The signal is collected on a multichannel scalar with the time zero for data acquisition set to the midpoint of the ion gate trigger. Mobility is determined according to eq 3 by plotting t_d versus P/V. The slope of the linear plot is inversely proportional to the reduced mobility, and the intercept equals the time spent within the second quadrupole before the detection of the ions. In most cases, this technique gives less than 1% standard deviation for repeated measurements.

III. Results and Discussion

A. Injection of $C_6H_6^+$ into Pure Helium and into a Benzene/Helium Mixture. Parts a and b of Figure 2 display the mass spectra obtained following injections of $C_6H_6^+$ ions, generated by 70-eV EI ionization, into the drift cell containing 2.0 Torr of pure He and 1.0×10^{-4} Torr of benzene in 2.0 Torr of He, respectively. It is clear that in the presence of neutral benzene in the cell the only product observed is the dimer cation $(C_6H_6)_2^+$, as expected. Therefore, on the basis of the mass spectrum alone, one could wrongly conclude that only two ionic species (monomer/dimer) are present with no evidence of additional species that may influence the measured equilibrium.

Figure 3a displays the ATD of $C_6H_6^+$ in pure He, and parts b and c of Figure 3 show the ATDs of $(C_6H_6)^+_2$ and $C_6H_6^+$, respectively, in a benzene/He mixture containing a small concentration of benzene (1.0×10^{-4} Torr). In the presence of benzene in the cell, the ATD of $C_6H_6^+$ clearly contains two separate components with the second peak arriving at almost the same time as the dimer peak. This indicates that the second peak represents reacting benzene cations, resulting in the formation of $(C_6H_6)^+_2$ dimer ions. It also suggests the presence of a $C_6H_6^+$ isomer that does not readily react with neutral benzene to form a dimer. This $C_6H_6^+$ isomer (denoted X^+) could

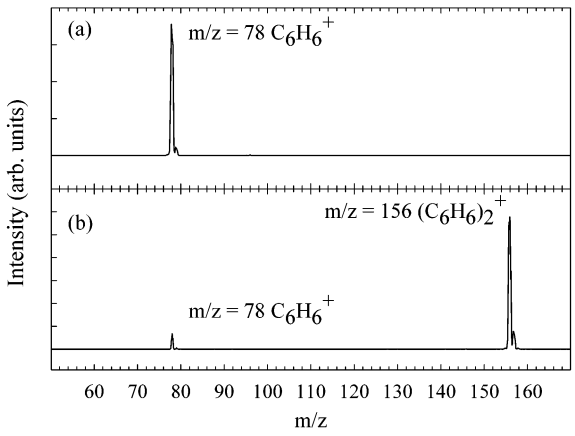

Figure 2. Mass spectra obtained following the injection of $C_6H_6^+$ into the drift cell containing (a) 2 Torr of pure helium at 304 K and (b) 1.0×10^{-4} Torr of benzene in 2 Torr of helium at 304 K.

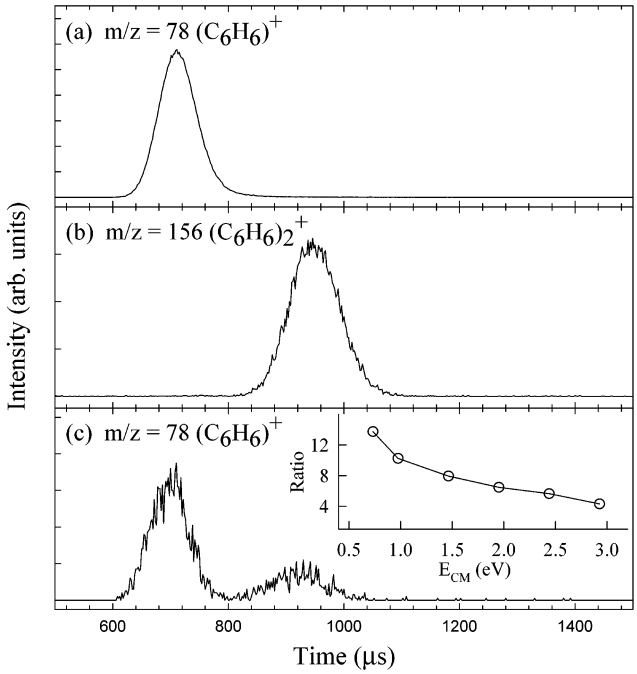

Figure 3. Arrival-time distributions of (a, c) $C_6H_6^+$ and (b) $(C_6H_6)_2^+$ measured following the injection of $C_6H_6^+$ into the drift cell containing (a) 2 Torr of pure helium at 304 K and (b, c) 1×10^{-4} Torr of benzene in 2 Torr of helium at 304 K. The inset in c shows the dependence of the percentage of ion intensity of the fulvene isomer relative to the total ion intensity (fulvene + benzene + benzene dimer) as a function of the injection energy of the of $C_6H_6^+$ ion. (E_{CM} is calculated with respect to the $C_6H_6^+$/He center-of-mass collision.[33])

have been generated by the EI ionization of benzene and simultaneously injected with the benzene cation into the cell. Alternatively, the X^+ isomer could have been formed inside the cell as a result of the ion injection process. As the ions are injected into the drift cell, the injection energy is dissipated in collisions with the He buffer gas. During this process, some of the kinetic energy can be converted into internal energy, heating the injected ions, and this may cause the ions to isomerize or fragment. In this case, one expects that increasing the injection energy of the $C_6H_6^+$ ions would increase the fraction of X^+ formed inside the cell. However, the data displayed in the inset of Figure 3c indicates that as the injection energy of the $C_6H_6^+$ ions increases (the injection energy, E_{CM}, is calculated with respect to the $C_6H_6^+$/He center-of-mass collision)[33] the fraction of X^+ formed decreases. This suggests that the increased injection energy is used to convert isomer X^+ into the most stable benzene cation. However, it is important to note that the data shown in the inset of Figure 3c provides only a qualitative trend of the effect of the injection energy on the relative amount of isomer X^+ that survived the injection process.

There are a large number of possible $C_6H_6^+$ isomers with at least 10 isomeric structures accessible below the lowest-energy dissociation limit for the benzene cation.[34−43] A possible rearrangement of the benzene cation generated by EI involves ring contraction to form fulvene (5-methylene-1,2-cyclopentadiene), which has the second lowest heat of formation next to the benzene cation.[35,36] The isomerization of the benzene ion to the fulvene structure is slightly endothermic (51 kJ/mol, 12.2 kcal/mol).[44−46] The results shown in Figure 3 could be explained by the generation of the fulvene cation as the X^+ isomer during the EI ionization of benzene in the ion source. In this case, the $C_6H_6^+$ ions injected into the drift cell consist of a mixture of benzene and fulvene cations. As the injection energy increases, more fulvene cations isomerize into the benzene cations. Semiempirical calculations of the isomerization of $C_6H_6^+$ show that the fulvene ions can rearrange to the benzene structure without decomposition.[42] The barrier for this isomerization, estimated to be 3.0 eV, is below the dissociation limit of 3.88 eV of the benzene cation.[42]

Our results indicate that the fraction of fulvene$^{+\bullet}$/benzene$^{+\bullet}$ decreases rather than increases with injection energy. This suggests that collisions with helium activate some of the injected fulvene$^+$ ions to isomerize to benzene$^+$. This observation suggests that fulvene$^+$ is formed during the EI ionization of benzene in the ion source rather than by collisions with helium atoms during ion injection.

The present observations can be used to obtain a lower limit to the barrier for the fulvene$^+$-to-benzene$^+$ isomerization. By measuring the ATD of the fulvene peak at higher temperatures in the drift cell, we found that even at the highest temperatures applied, 453 K, at least 80% of the injected fulvene$^+$ ions survived the drift time of 1.3 ms in the drift cell. Therefore, the rate coefficient $k(T = 453\ \text{K}) < 171.6\ \text{s}^{-1} = A \exp(-E_a/RT)$. Assuming a usual A factor of $10^{14}\ \text{s}^{-1}$, this observation yields an activation energy E_a(fulvene$^+ \rightarrow$ benzene$^+$) > 24.3 kcal/mol, and assuming an A factor between 10^{13} and $10^{15}\ \text{s}^{-1}$ yields $E_a > 22.2$ and 26.4 kcal/mol, respectively. Considering the 12.2 kcal/mol difference between $\Delta H°_f$(benzene$^+$) and $\Delta H°_f$(fulvene$^+$), our results yield E_a(benzene$^+ \rightarrow$ fulvene$^+$) > 36.5 kcal/mol. Assuming A factors between 10^{13} and $10^{15}\ \text{s}^{-1}$ yields the lower limit to be between 34.4 and 38.6 kcal/mol.

It is interesting that the ATD of $C_6H_6^+$ in pure helium is characterized by a single peak, which indicates that the collision cross sections of the benzene and X cations are not sufficiently different in pure helium to provide different drift velocities under the current resolution of our drift cell. However, the great difference in the reactivity of the benzene and X cations toward the association with neutral benzene leads to an efficient separation between the two isomers in the presence of neutral benzene in the cell. This observation is entirely consistent with the work of Gross and co-workers,[44−46] who found that under ICR conditions (10^{-6} to 10^{-4} Torr, electron ionization energies between 10 and 25 eV) no condensation products were observed between ionized fulvene ($C_6H_6^+$) and neutral C_6D_6. The only ion−molecule reaction that was found was the charge-exchange reaction of a benzene radical cation ($C_6D_6^+$) with a fulvene neutral (C_6H_6) because the ionization potential (IP) of fulvene (8.36 eV) is <IP of benzene (9.25 eV).[44−47]

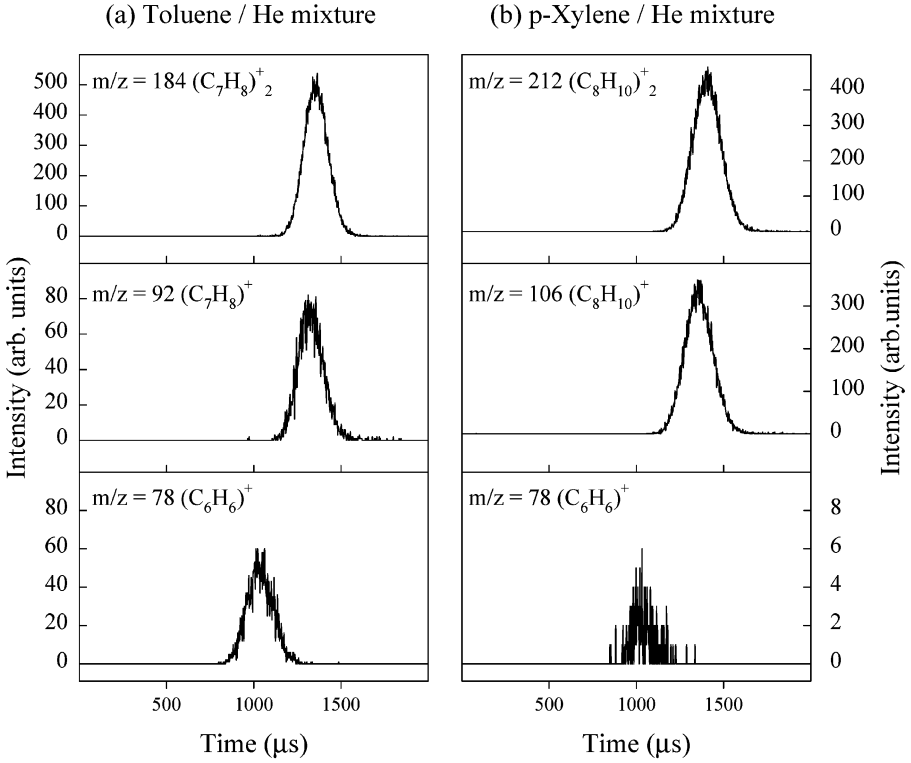

Figure 4. Arrival-time distributions measured following the injection of $C_6H_6^+$ into the drift cell containing (a) 1.5×10^{-2} Torr of toluene in 2 Torr of helium at 304 K and (b) 2.5×10^{-2} Torr of *p*-xylene in 2 Torr of helium at 304 K. Note that the $C_6H_6^+$ peak in b has almost negligible intensity.

B. Identification of the X^+ Isomer via the Ionization Potential. To support the assumption that the observed nonreactive (toward neutral benzene) X^+ isomer of $C_6H_6^+$ is in fact the fulvene ion, we carried out a series of experiments designed to bracket the IP of the neutral precursor of X^+. In these experiments, the 70-eV EI $C_6H_6^+$ ions were injected into the drift cell containing a known concentration of toluene or *p*-xylene in helium. The ATDs of the resulting ions in the toluene and *p*-xylene experiments are shown in parts a and b of Figure 4, respectively. Because the IP of benzene (9.25 eV) is higher than that of toluene (8.83 eV),[47] the injected benzene cations undergo exothermic charge-transfer reactions with neutral toluene, thus producing the toluene cations ($C_7H_8^+$) as shown in Figure 4a. The $C_7H_8^+$ cations undergo efficient association with neutral toluene molecules, thus forming toluene dimer cations $(C_7H_8)^+_2$, as expected. However, a significant number of $C_6H_6^+$ ions are left unreacted in the 78 *m*/*z* mass channel, indicating that these ions (X^+ isomer) correspond to a neutral precursor with a lower IP than toluene. In the presence of *p*-xylene in the cell, almost all of the X^+ isomer ions undergo efficient charge transfer to produce *p*-xylene ions ($C_8H_{10}^+$), which then generate the *p*-xylene dimer cation as a result of the association with the neutral molecules, as shown in Figure 4b. The negligible number of X^+ isomer ions left in the 78 *m*/*z* mass channel in Figure 4b indicates that the IP of the neutral precursor of the X^+ isomer must be very close to that of *p*-xylene (8.44 eV).[47] Indeed, the injection of $C_6H_6^+$ ions into the drift cell containing a known concentration of triethylamine (TEA, IP = 7.53 eV)[47] in helium showed that all of the $C_6H_6^+$ ions (benzene and X cations) reacted by charge transfer to generate TEA ions. This result confirms that the IP of the neutral precursor of the X^+ isomer must lie between 7.53 and 8.44 eV but much closer to 8.44 eV. This is consistent with the assignment of the fulvene cation to the X^+ isomer.

TABLE 1: Comparison between the Measured Reduced Mobilities and the Literature Values

ion	K_0 (this work) $cm^2\ V^{-1}\ s^{-1}$	K_0 (literature) $cm^2\ V^{-1}\ s^{-1}$	ref
Ar^+	20.5 ± 0.8	$20.3 \pm 5\%$	48
H_2O^+	21.0 ± 0.8	$20.8 \pm 5\%$	49
$H_3O^+ \cdot (H_2O)$	17.5 ± 0.6	$17.3 \pm 5\%$	49
$H_3O^+ \cdot (H_2O)_2$	13.6 ± 0.5	$13.8 \pm 5\%$	49
$H_3O^+ \cdot (H_2O)_3$	11.1 ± 0.4		
$C_6H_6^+$	11.4 ± 0.4	11.8 ± 0.3	50
$C_5H_5N^+$	11.7 ± 0.4		
triethylamine$^+$	8.4 ± 0.4		
p-xylene$^+$	9.1 ± 0.4		
CS_2^+	14.4 ± 0.5		

C. Identification of the X^+ Isomer by Ion Mobility. Further support for the $C_6H_6^+$ isomer assignment can be obtained from the measured ion mobility, which is directly related to the collision cross section of the ion with the buffer gas. As a check of our new instrument for the mobility measurements, we measured the mobility of several atomic, molecular, and cluster ions. The results along with the literature values are shown in Table 1. The agreement between our measured mobilities and the literature values is very good,[48−50] well within the estimated errors.

The mobility of the benzene cation $(C_6H_6)^+$ was measured several times with the source operated in both continuous- and pulsed-beam modes using a 10-μs ion gate width. Figure 5a shows a typical ATD of the mass-selected $C_6H_6^+$ ions injected into pure helium, and Figure 5b illustrates the variation of the ATDs with $^P/_V$ used to calculate the mobility of $C_6H_6^+$. The data shown in Figure 5c yields a slope of $(8.22 \pm 0.04) \times 10^{-3}$ (s V/Torr) and an intercept of $33 \pm 3\ \mu$s. The repeated mobility measurements yield a reduced mobility for the benzene cation of $K_0 = 11.4 \pm 0.1\ (0.2)\ cm^2\ V^{-1}\ s^{-1}$; the uncertainty given here is ± 1 standard deviation in the repeated measurements,

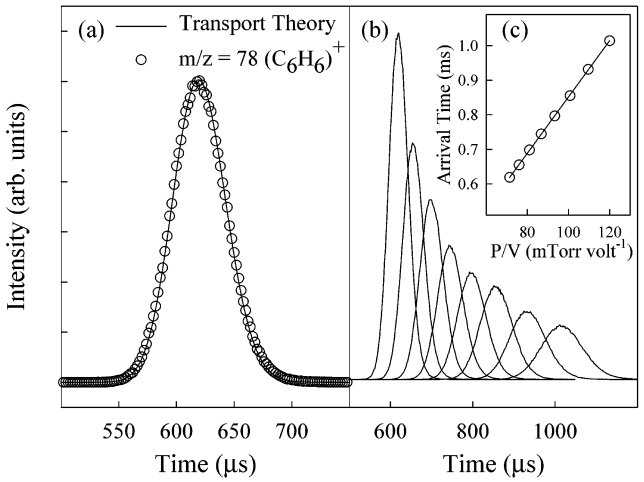

Figure 5. (a) Comparison of the ATD of $C_6H_6^+$ in pure helium (2.5 Torr, $^{E}/_{N} = 4.9$ Td) with the prediction of transport theory (eq 4). (b) ATDs of $C_6H_6^+$ at different drift voltages (decreasing from left to right). (c) Plot of the mean arrival time (t_0) of $C_6H_6^+$ as a function of $^{P}/_{V}$ (Torr V^{-1}).

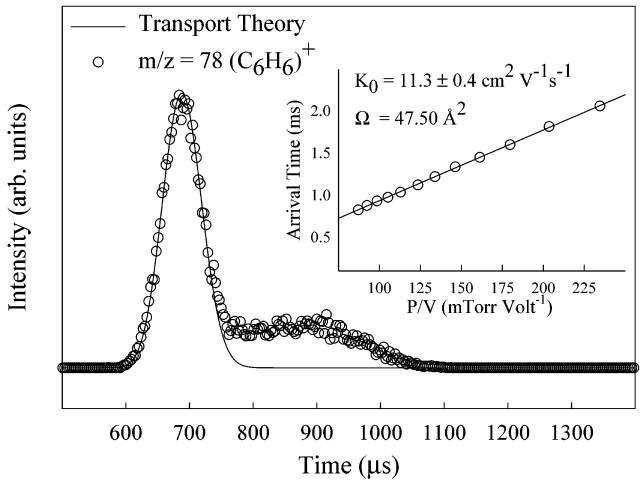

Figure 6. Comparison of the ATD of the $C_6H_6^+$ peak corresponding to the fulvene isomer (first peak at shorter time) with the prediction of transport theory (eq 4) using the calculated collision cross section of the fulvene structure ($P = 2.7$ Torr, $^{E}/_{N} = 4.6$ Td). The inset shows a plot of the mean arrival time (t_0) of $C_6H_6^+$ (fulvene peak) as function of $^{P}/_{V}$.

and the value in parentheses represents a 2% estimated error in the mobility measurements.

The measured ATD can be calculated from the transport equation for a short packet (δ pulse) of ions injected into a cylindrical drift tube through an aperture of area a using eq 4.[32,51]

$$\phi(t) = \frac{sae^{-\alpha t}}{4\sqrt{\pi D_L t}}\left(v_d + \frac{l}{t}\right)\left(1 - \exp\left(-\frac{r_0^2}{4D_T t}\right)\right)\exp\left(-\frac{(l - v_d t)^2}{4D_L t}\right) \quad (4)$$

The ions are introduced as a δ pulse in the form of an axially thin disk of radius r_0 and uniform surface density s. The loss of ions through reactions during the drift time can be accounted for through frequency factor $\tilde{\alpha}$. D_L and D_T are the longitudinal and transverse diffusion coefficients, respectively, which (under low-field conditions) are related to the mobility by the Einstein equation:[51]

$$D_L = D_T = K\frac{k_B T}{ze} \quad (5)$$

where ze is the number of charges times the charge of the electron.

A comparison of the measured ATD of the $C_6H_6^+$ ions with the prediction from transport theory using eq 4 is shown in Figure 5a. The agreement between the measured and predicted ATDs may suggest that the ATD peak of the $C_6H_6^+$ ions consists of one isomer. However, the resolution of isomers is limited by the diffusion of the ion packet as it travels through the drift tube. If two isomers have mobilities that differ by less than the ion packet expands, then they will not be resolved.[52] This appears to be the case for the $C_6H_6^+$ ions where a fraction of the X isomer ions is produced by EI along with the benzene cations. As mentioned before, the separation between the X isomer and benzene cations is enhanced in the presence of neutral benzene because of the different reactivity of the X isomer and benzene cations toward the association with neutral benzene molecules. This suggests that isomer ions with similar mobilities can be separated on the basis of the degree of their associations with the neutral precursor in the drift cell. This separation concept allows us to discover the "hidden isomerization" process responsible for the generation of fulvene cations by the EI ionization of benzene.

Because the X isomer can be separated from benzene cations in the presence of a small concentration of neutral benzene in the drift cell, it is possible to measure the mobility of the X isomer under these conditions. From the variations of the ATD of the X isomer peak with $^{P}/_{V}$, the reduced mobility of the X^+ isomer was calculated as 11.2 ± 0.2 cm^2 V^{-1} s^{-1} as shown in Figure 6. This measured mobility was corrected for the fact that the ions were drifting in a mixture of benzene and helium using Blanc's law.[32,51] Because the X isomer cations are not involved in the association and dissociation reactions that form and remove the benzene dimer cation, these reactions are not expected to influence the measured mobility of the X isomer cation.

Structural information on the X^+ isomer can be obtained by comparing the measured $\Omega(X^+)$ with calculated cross sections for low-energy isomers of $C_6H_6^+$ ions. According to kinetic theory,[53] the mobility of an ion is related to the average collision cross section of the ion with the buffer gas by eq 8.[49,51]

$$K = \frac{1}{N}\frac{(18 \cdot \pi)^{1/2}}{16}\left[\frac{1}{m} + \frac{1}{m_b}\right]^{1/2}\frac{z \cdot e}{(k_B \cdot T)^{1/2} \cdot \Omega^{(1,1)}_{avg}} \quad (6)$$

where N is the buffer gas number density, m is the mass of the ion, m_b is the mass of a buffer gas atom, z is the number of charges, e is the electron charge, k_B is Boltzmann's constant, and $\Omega^{(1,1)}_{avg}$ is the average collision integral. Using eq 6 and the measured mobility of the X^+ isomer, the average collision cross section in helium, $\Omega(X^+)$, was calculated as 47.5 Å^2.

The heats of formation of five low-energy isomers of the $C_6H_6^+$ ions along with the ionization potentials of the corresponding neutral molecules are listed in Table 2. The lowest-energy structures of four isomer cations, namely, benzvalene, fulvene, 4,4-dimethylcyclobut-1-ene, and 1,5-hexadien-3-yne, were obtained using ab initio calculations at the UHF/6-31+G-(d,P) level of theory.[54] The calculated structures were used to obtain average collision cross sections using the hard sphere scattering model, the projection approximation, and the trajectory calculations,[25,27] and the results are included in Table 2. As pointed out by Jarrold, the cross sections determined from

(a) Benzvalene	(b) Fulvene	(c) 3,4-Dimethylcyclobut-1-ene	(d) 1,5-Hexadien-3-yne
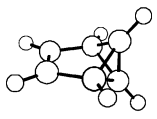	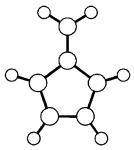	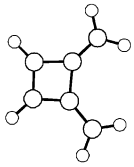	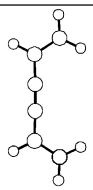
$\Omega = 46.260$ Å^2	$\Omega = 48.308$ Å^2	$\Omega = 49.839$ Å^2	$\Omega = 53.112$Å^2
$K_o = 11.8$ cm^{2}V^{-1}s^{-1}	$K_o = 11.3$ cm^{2}V^{-1}s^{-1}	$K_o = 10.9$ cm^{2}V^{-1}s^{-1}	$K_o = 10.2$ cm^{2}V^{-1}s^{-1}

Figure 7. Ab initio structures of the $C_6H_6^+$ isomers obtained at the UHF/6-31+G(d,P) level, the corresponding cross sections calculated using the trajectory method,[25] and the reduced mobilities.

TABLE 2: ΔH^0_f, Ionization Energies, and Calculated Collision Cross Sections[a] of Selected $C_6H_6^+$ Isomers

$C_6H_6^+$ isomer	ΔH^0_f, kJ mol^{-1} (kcal/mol)[35]	ionization energy (eV)[47]	Ω, (Å^2) (calculated) [25]		
			HS	proj	traj
benzene	993 (237.6)	9.24	50.32	49.28	47.14
fulvene	1044 (249.8)	8.36	51.67	50.46	48.31
benzvalene	1163 (278.2)	8.1	49.41	48.38	46.26
dimethylcyclobutene	1177 (281.6)	8.8	53.48	51.96	49.84
1,5-hexadien-3-yne	1189 (284.4)	8.5	57.57	55.79	53.11

[a] Using hard spheres (HS), projection (proj), and trajectory (traj) methods.[25]

the exact hard sphere scattering model are within a few percent of those obtained from trajectory calculations.[27] The calculated UHF/6-31+G(d,P) structures of the four isomers along with the cross sections obtained from the trajectory method are shown in Figure 7. It is clear that the fulvene structure results in a cross section (48.3 Å^2) that matches the experimental cross section measured for isomer X (47.5 Å^2). The same conclusion can be reached by using the calculated mobility of the fulvene cation to fit the measured ATD of the X^+ isomer to the transport equation (eq 4). The calculated ATD, as shown in Figure 6, is in excellent agreement with the measured ATD for X^+. This provides further confirmation of the assignment of the fulvene structure to the X^+ isomer.

To demonstrate that the ATDs of the fulvene and benzene ions in pure helium are not resolvable, we constructed a composite ATD peak consisting of a 90:10 mixture of benzene and fulvene ions (similar to the experimentally measured ratio) using the calculated cross sections from the trajectory method. As shown in Figure 8a, only one peak is present, almost identical to the pure benzene ion peak, in full agreement with the experimental ATD shown in Figure 3a. However, if X^+ is another isomer of $C_6H_6^+$, which has a sufficiently different cross section than benzene$^+$, then a second peak should be observed in the ATD of $C_6H_6^+$. This is clearly shown in the composite ATDs (shown in Figure 8b) constructed for a 90:10 mixture of benzene and 1,5-hexadien-3-yne ions using the calculated cross sections from the trajectory method. In contrast to the experimental ATD (Figure 3a), the 90:10 mixture of benzene and 1,5-hexadien-3-yne ions exhibits ATDs consisting of two peaks as shown in Figure 8b.

D. Isomerization by Exothermic Charge-Transfer Reactions in the Drift Cell. The effect of generating benzene cations inside the drift cell was investigated by injecting mass-selected Ar^+ and CS_2^+ into the drift cell containing a benzene/helium mixture. The mass spectra and ATDs resulting from the injections of Ar^+ and CS_2^+ ($E_{CM} = 0.91$ and 0.50 eV, calculated with respect to the Ar^+/He and CS_2^+/He center-of-mass collisions, respectively)[33] are shown in parts a and b of Figure 9,

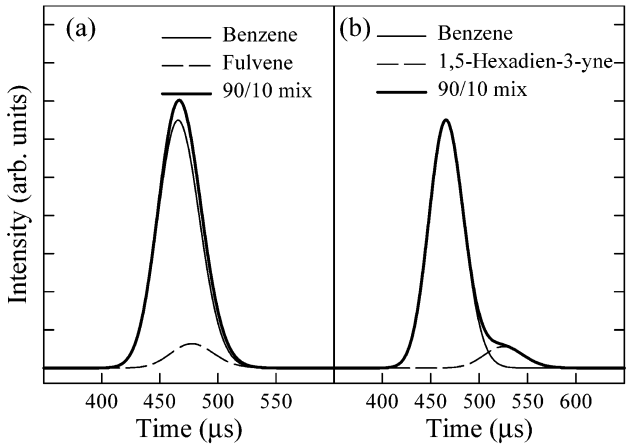

Figure 8. (a) Composite theoretical ATD of a (90:10) benzene$^+$/fulvene$^+$ mixture obtained using the calculated cross sections of both ions. (b) Composite theoretical ATD of a (90:10) benzene$^+$/1,5-hexadien-3-yne$^+$ mixture obtained using the calculated cross sections of both ions.

respectively. It is clear that the exothermic charge-transfer reaction between Ar^+ and benzene ($\Delta IP = 6.6$ eV)[47] results in significant fragmentation of the benzene cation. The ATDs shown in Figure 9a indicate that the fulvene cation has been produced along with the benzene cation, similar to the results obtained by injecting the $C_6H_6^+$ ions produced by EI. The observation of the fulvene cation simultaneously with benzene ion fragmentation indicates that ionized benzene must isomerize to other structures prior to or concurrent with dissociation. This is consistent with the well-known result that ionized benzene sufficiently activated to decompose shows a strong propensity for carbon and hydrogen scrambling.[45,55,56] However, the injection of CS_2^+ ($E_{CM(CS_2^+/He)} = 0.5$ eV) into the drift cell does not result in the formation of benzene fragments as shown in Figure 9b. This is due to the small ΔIP between CS_2 and benzene (0.6 eV),[47] which is not sufficient to induce the dissociation of the benzene cation. The ATDs also indicate that no X^+ (fulvene) isomer is formed at the $E_{CM(CS_2^+/He)} = 0.5$ eV injection energy of CS_2^+. This shows that the injection energy is dissipated in collisions with the helium buffer gas and not enough energy is available to overcome the barrier to the benzene$^{+\bullet} \rightarrow$ fulvene$^{+\bullet}$ isomerization. However, by increasing the injection energy of CS_2^+, isomerization may take place as shown in the inset of Figure 9b, which demonstrates the increase in the fraction of the fulvene isomer produced with higher injection energies of CS_2^+.

It is interesting that increasing the injection energies of the C_6H_6 ions (being a mixture of benzene and fulvene cations) results in the isomerization of fulvene to the more stable benzene

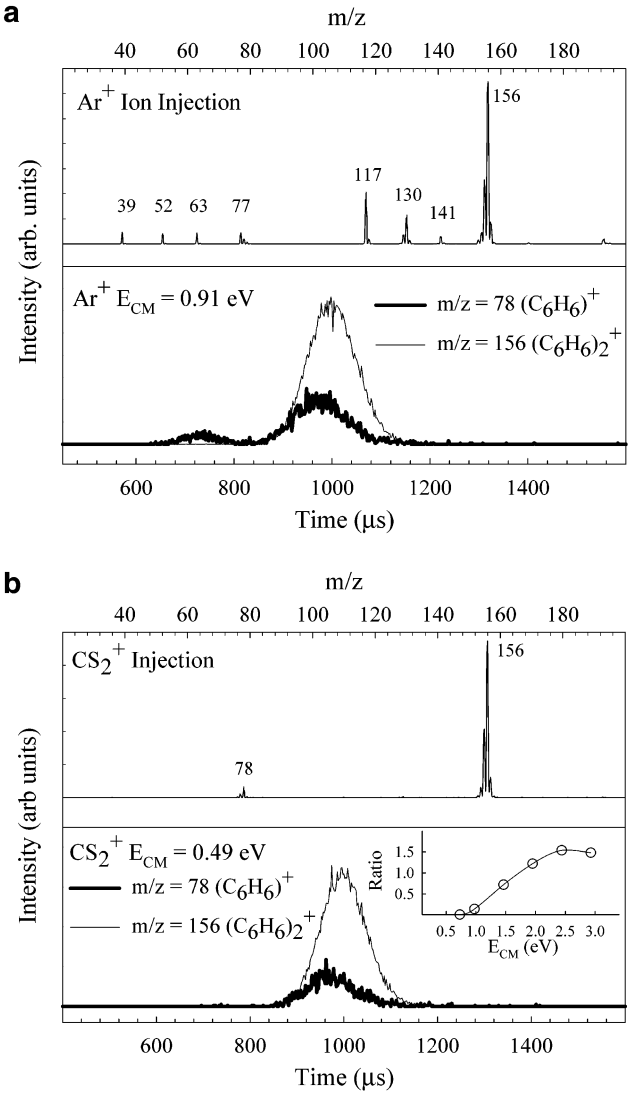

Figure 9. (a) (Top) Mass spectrum resulting from the injection of Ar^+ ($E_{CM} = 0.49$ eV) into the drift cell containing 1.0×10^{-4} Torr of benzene in 2 Torr of helium at 304 K. (Bottom) ATD of the $C_6H_6^+$ ions (two peaks) and $(C_6H_6)_2^+$ ion (one peak). (b) (Top) Mass spectrum resulting from the injection of CS_2^+ into the drift cell containing 1.0×10^{-4} Torr of benzene in 2 Torr of helium at 304 K. (Bottom) ATD of the $C_6H_6^+$ ions (one peak) and $(C_6H_6)_2^+$ ion (one peak) obtained following the injection of CS_2^+ ($E_{CM} = 0.49$ eV) into the drift cell containing 1.0×10^{-4} Torr of benzene in 2 Torr of helium at 304 K. The inset shows the dependence of the percentage of ion intensity of the fulvene isomer relative to the total ion intensity (fulvene + benzene + benzene dimer) as a function of the injection energy of the CS_2^+ ion (E_{CM}, in eV).

cations (inset of Figure 3c). However, increasing the injection energies of CS_2^+ ions increases the fraction of fulvene cations produced from exothermic charge-transfer reactions to neutral benzene molecules inside the drift cell (inset of Figure 9b).

E. Measurements of the Binding Energies of the Benzene Dimer Cation. The above results establish that exothermic charge transfer produces rearranged C_6H_6 ions (fulvene) that are nonreactive toward benzene neutrals and result in a constant, time-independent ratio that may appear as equilibrium. The effect of fulvene on the measured equilibrium constant of the benzene dimer cation increases as the equilibrium concentration of the benzene cation decreases at lower temperatures. However, the concentration of the nonreactive C_6H_6 isomer (fulvene) becomes negligible when charge transfer to C_6H_6 occurs from CS_2 with low injection energy.

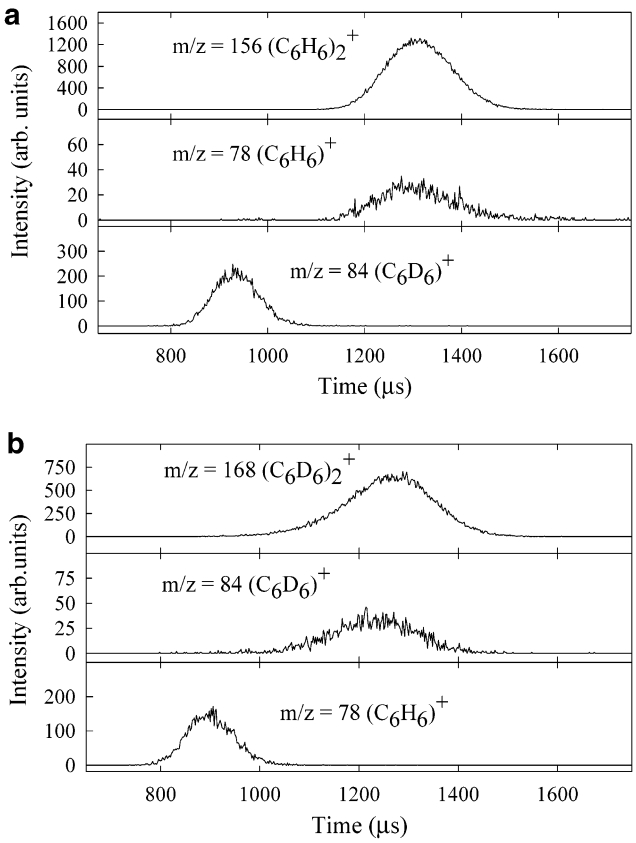

Figure 10. (a) Arrival-time distributions of $C_6D_6^+$ (fulvene cation), $C_6H_6^+$ (benzene cation), and $(C_6H_6)_2^+$ (benzene dimer cation) measured following the injection of $C_6D_6^+$ into the drift cell containing 5.5×10^{-2} Torr of C_6H_6 in 2.0 Torr of helium at 353 K. **(**b) Arrival-time distributions of $C_6H_6^+$ (fulvene cation), $C_6D_6^+$ (benzene cation), and $(C_6D_6)_2^+$ (benzene dimer cation) measured following the injection of $C_6H_6^+$ into the drift cell containing 5.3×10^{-2} Torr of C_6D_6 in 2.0 Torr of helium at 323 K.

To measure the equilibrium constant for the formation of the benzene dimer cation with no interference from the fulvene cations, we took advantage of the similarity between the IPs of C_6H_6 and C_6D_6.[20] From the results of high-n Rydberg spectroscopy,[57] the IP of C_6D_6 (9.247 eV) is slightly higher than that of C_6H_6 (9.244 eV). This very small difference in the IPs does not affect the charge-transfer resonance between benzene-h_6 and benzene-d_6 because the intensity of the charge-resonance (CR) band of HD^+ was found to be similar to that of H_2^+.[58] This means that by injecting $C_6D_6^+$ ions ($m/z = 84$) into the drift cell containing a benzene (C_6H_6)/helium mixture, the fraction of $C_6D_6^+$ present as fulvene cations would not undergo charge transfer to C_6H_6 (IP of fulvene = 8.35 eV). Therefore, the ion signal present in the $m/z = 84$ mass channel would correspond to fulvene cations, and the $m/z = 78$ ion signal would correspond to benzene cations. Using this technique, the equilibrium between $C_6H_6^+$ and $(C_6H_6)_2^+$ was clearly established, as indicted by the identical ATDs of the $C_6H_6^+$ and $(C_6H_6)_2^+$ ions shown in Figure 10a. The same strategy was applied to measure the equilibrium constant for the formation of $(C_6D_6)_2^+$ by injecting $C_6H_6^+$ ($m/z = 78$) into a C_6D_6/He mixture. Examples of the ATDs of the $C_6H_6^+$, $(C_6H_6)_2^+$ and the $C_6D_6^+$, $(C_6D_6)_2^+$ ions under equilibrium conditions are shown in parts a and b of Figure 10, respectively. All of the equilibrium measurements were carried out with $E/n < 3$. As described in the Experimental Section, the measured equilibrium constant was independent of the applied field across the drift cell in the low-field region. The equilibrium constant measured

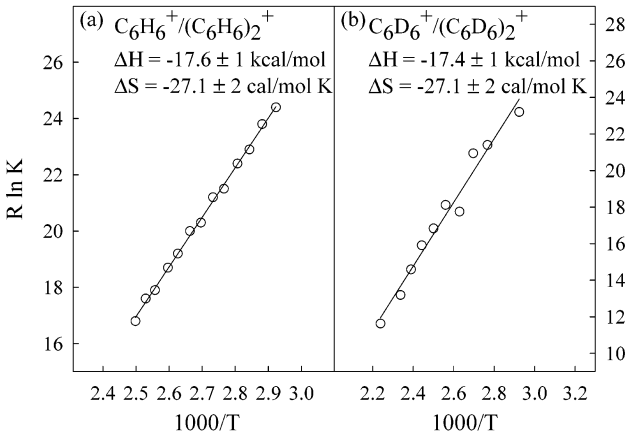

Figure 11. van't Hoff plots for the formation of benzene dimer cations (a) $(C_6H_6)_2^+$ and (b) $(C_6H_6)_2^+$.

as a function of temperature yields $\Delta H°$ and $\Delta S°$ from the van't Hoff equation:

$$\ln K = -\frac{\Delta H°}{RT} + \frac{\Delta S°}{R} \tag{7}$$

Typical van't Hoff plots for the formation of $(C_6H_6)_2^+$ and $(C_6D_6)_2^+$ are shown in Figure 11. All of the results were reproduced at least three times. The slopes of the plots yield $\Delta H° = -17.6 \pm 1$ and -17.4 ± 1 kcal/mol for bonding enthalpies of $(C_6H_6)_2^+$ and $(C_6D_6)_2^+$, respectively. The intercepts yield $\Delta S° = -27 \pm 2$ cal/mol K and -27 ± 2 cal/mol K, respectively, for entropy changes of formation for $(C_6H_6)_2^+$ and $(C_6D_6)_2^+$, respectively. These results are in excellent agreement with the values reported by Meot-Ner et al.[11] and are smaller than the values measured by Hiraoka and co-workers.[17]

Although our results confirm the $\Delta H°$ value for the formation of $(C_6H_6)_2^+$ as measured by Meot-Ner et al.,[11] we are not able to explain the reasons for the higher $\Delta H°$ value obtained by Hiraoka et al.[17] From the present results, it appears that if fulvene$^+$ ions were present in the previous experiments then a lower $\Delta H°$ value rather than a higher value would have been obtained.

F. Applications to Proton-Bound Dimers. *Measurements of the Binding Energies of H^+(Pyridine)$_2$ and H^+(Triethylamine)$_2$.* To compare the measured binding energy of the benzene dimer cation with those of proton-bound dimers, we measured the equilibrium constants for the formations of H^+(pyridine)$_2$ and H^+(triethylamine)$_2$ as a function of temperature. These systems are characterized by stronger bonding interactions compared to those of the benzene dimer cation. Figure 12a shows the mass spectra measured following the injection of mass-selected pyridine cations ($C_5H_5N^+$, produced by EI ionization of pyridine) into the drift cell containing pure helium and a pyridine/helium mixture. The $C_5H_5N^+$ ions undergo the well-known proton-transfer reaction with neutral pyridine molecules in the cell to generate the $C_5H_5NH^+$ ions, which react further to form the protonated dimer $H^+(C_5H_5N)_2$. Equilibrium conditions were easily established at higher temperatures, as evident from the ATDs of the $C_5H_5NH^+$ and $H^+(C_5H_5N)_2$ ions displayed in Figure 12b. The van't Hoff plot resulting from the measured equilibrium constants at different temperatures is shown in Figure 12c. From the slope and intercept, $\Delta H° = -25.2 \pm 1$ kcal/mol and $\Delta S° = -29.7 \pm 2$ cal/mol K for the formation of $H^+(C_5H_5N)_2$ are determined. These values are in excellent agreement with $\Delta H° = -25.2$ kcal/mol and $\Delta S° = -29.6$ cal/mol K measured by Meot-Ner using pulsed high-pressure mass spectrometry.[59] Our values are also consistent with earlier measurements from several laboratories that reported $-\Delta H° = 24.6$,[60] 23.7,[61] and 26.3[62] kcal/mol and $-\Delta S° = 28.2$,[60] 28.0,[61] and 32.1[62] cal/mol K.

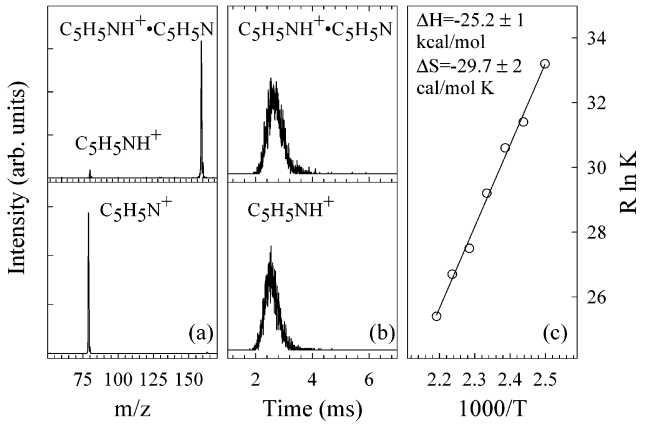

Figure 12. (a) Mass spectra obtained following the injections of $C_5H_5N^+$ into the drift cell containing 2.0 Torr of pure helium at 303 K (bottom) and 8.4×10^{-4} Torr of pyridine in 3.6 Torr of helium at 400 K (top). (b) Arrival-time distributions of $C_5H_5NH^+$ and $(C_5H_5N)_2H^+$ at 7.6×10^{-4} Torr of pyridine in 3.6 Torr of helium at 438 K. (c) van't Hoff plot for the formation of the proton-bound pyridine dimer.

A comparison between the binding energies in the benzene dimer cation and in the proton-bound pyridine dimer reveals that a significant difference exists in the magnitude of binding. This may be explained by the different nature of intermolecular interactions in the two systems. The bonding in these systems results from a combination of electrostatic, polarization, dispersion, and short-range repulsion. However, in the proton-bound dimer, the electrostatic interaction is the dominant term contributing to the binding through the strong ionic hydrogen-bonding interaction. However, charge resonance may contribute significantly to the binding in the benzene dimer cation. This contribution has been estimated as being up to 30% of the total binding energy in aromatic dimer cations exhibiting sandwich structures (i.e., the two molecules are parallel), which maximize the charge-resonance interaction.[63,64] Considering that the dispersion interaction may be of similar magnitude in the benzene dimer cation and the protonated pyridine dimer, one may estimate the strength of the ionic hydrogen bond as twice the charge-resonance stabilization in aromatic dimer cations.

Figure 13a displays the mass spectra obtained following the injection of triethylamine (TEA) cations $(C_2H_5)_3N^+$, produced by EI ionization of TEA, into the drift cell containing pure helium and a TEA/helium mixture. In pure helium, the $(C_2H_5)_2NCH_2^+$ion, ($m/z = 86$) is observed as a result of CH_3 loss from the $(C_2H_5)_3N^+$ ion upon injection. In the presence of TEA in the drift cell, a proton-transfer reaction produces the $(C_2H_5)_3NH^+$ ion ($m/z = 102$), which then undergoes association with neutral TEA to form proton-bound dimer $[(C_2H_5)_3N]_2H^+$ ($m/z = 203$). In addition, elimination reactions producing $(C_2H_5)_3NH^+NCH_3(C_2H_5)_2$ ($m/z = 189$), $(C_2H_5)_3N^+NCH_2(C_2H_5)_2$ ($m/z = 187$), $(C_2H_5)_3NH^+N(CH_3)_2(C_2H_5)$ ($m/z = 175$), and $(C_2H_5)_3N^+N(C_2H_5)_2$ ($m/z = 173$) are also observed. The attainment of equilibrium between $(C_2H_5)_3NH^+$ and $[(C_2H_5)_3N]_2H^+$ was verified as illustrated in Figure 13b from the identical ATDs measured for the two ions under equilibrium conditions. From the slope and intercept of the van't Hoff plot displayed in Figure 13c, $\Delta H° = -20.9 \pm 1$ kcal/mol and $\Delta S° = -42.7.1 \pm 2$ cal/mol K for the formation of $[(C_2H_5)_3N]_2H^+$ are determined. Our $-\Delta S°$ value is in excellent agreement with the value reported by Meot-Ner and Sieck[60] (41.0 cal/mol K), but their $-\Delta H°$ value

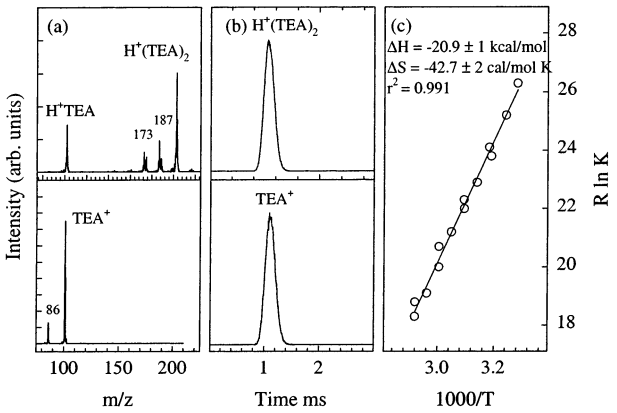

Figure 13. (a) Mass spectra obtained following the injections of $(C_2H_5)_3N^+$ into the drift cell containing 2.1 Torr of pure helium at 304 K (bottom) and 2.3×10^{-3} Torr of triethylamine in 2.0 Torr of helium at 304 K (top). (b) Arrival-time distributions of $(C_2H_5)_3N^+$ and $[(C_2H_5)_3N]_2H^+$ at 2.3×10^{-5} Torr of triethylamine in 2.1 Torr of helium at 318 K. (c) van't Hoff plot for the formation of the proton-bound triethylamine dimer.

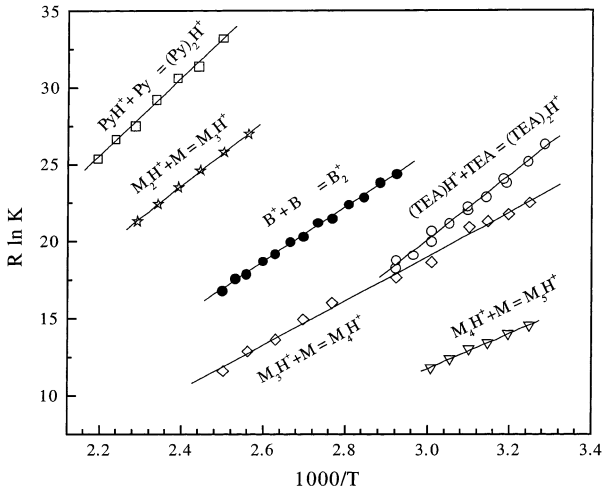

Figure 14. van't Hoff plots for the formation of protonated methanol clusters $(M_n)H^+$ with $n = 3-5$, the benzene dimer cation (B_2^+), the proton-bound pyridine dimer $[(Py)_2H^+]$, and the proton-bound triethylamine dimer $[(TEA)_2H^+]$.

$(23.8 \pm 1$ kcal/mol) is significantly higher than our value. However, it should be pointed out that the van't Hoff plot reported in ref 60 is based on only three measurements of the equilibrium constant in the temperature range of 385−435 K, and our data (Figure 13c) contains more than 10 measurements of the equilibrium constant over the temperature range of 300−350 K. The large entropy loss associated with the formation of $[(C_2H_5)_3N]_2H^+$ reflects the strong steric hindrance effects resulting from the six ethyl groups.[59]

G. Applications to Protonated Methanol Clusters $H^+(CH_3OH)_n$. Among the common factors contributing to the uncertainty in equilibrium measurements are the accurate determinations of the temperature and vapor concentration of the neutral molecules under equilibrium conditions where the dimer/monomer ion ratio is measured. To check further the accuracy of our mass-selected drift cell in obtaining thermochemical properties of ion clustering, we measured the thermochemistry of formation of the $H^+(CH_3OH)_n$ clusters with $n = 3-5$. The temperature range and binding energies in these protonated clusters extend below and above the temperature and binding-energy ranges of the benzene dimer cation. Our measurements yield $-\Delta H° = 21.0 \pm 0.7$, 14.3 ± 0.4, and 11.3 ± 0.4 kcal/mol for the $H^+(CH_3OH)_n$ clustering steps $(n-1 \rightarrow n)$ with $n = 3-5$, respectively. These values are in excellent agreement with literature values.[28−30] For comparison, the literature $\Delta H°$ values are 23.0,[28] 21.0,[29] and 21.3[30] kcal/mol for $n = 3$; 14.0[28] and 16.1[30] kcal/mol for $n = 4$; and11.3[28] and 13.5[30] kcal/mol for $n = 5$. Similarly, our measured $\Delta S°$ values (27.6 ± 1, 24.3 ± 1, and 22.2 ± 1.1 cal mol^{-1} K^{-1} for $n = 3-5$, respectively) are also in excellent agreement with literature values (25.8,[28] 25.8,[29] and 28.2[30] cal mol^{-1} K^{-1}for $n = 3$; 24.0[28] and 28.9[30] cal mol^{-1} K^{-1} for $n = 4$; and 22.3[28] and 28.7[30] cal mol^{-1} K^{-1} for $n = 5$.

Figure 14 displays the van't Hoff plots obtained using our mass-selected drift cell for the stepwise formation of $H^+(CH_3OH)_n$ clusters with $n = 3-5$ and for the formation of $(C_6H_6)_2^+$, $H^+(C_5H_5N)_2$, and $[(C_2H_5)_3N]_2H^+$. It is clear that our system produces results in agreement with literature values over wide ranges of temperature and binding energies. The results establish the validity of using our new drift cell instrument for measuring thermochemical properties of association reactions involving molecular cations and protonated molecules. The combination of thermochemical properties and structural information obtained by measuring the collision cross sections of the association product ions provides a unique opportunity to investigate the structure−property relationship in these systems.

IV. Summary and Conclusions

In this work, we have used a mass-selected, drift cell technique to (1) reveal the hidden isomerization process responsible for the generation of fulvene cations by the electron impact ionization of benzene; (2) estimate a lower limit to the barrier for the (fulvene$^{+\bullet}$ → benzene$^{+\cdot}$) isomerization (∼1.0 eV) by thermal activation at 453 K; (3) study the exothermic charge-transfer isomerization by selective injections of Ar^+ and CS_2^+ with variable injection energies; (4) measure the temperature dependence of the equilibrium constant for the formation of the benzene dimer cation in both the $(C_6H_6)_2^{+\bullet}$ and $(C_6D_6)_2^{+\bullet}$ systems without interference from the fulvene isomer ion; (5) measure the binding energies and entropy changes for the formation of proton-bound dimers in the pyridine and triethylamine systems; and (6) measure the binding energies and entropy changes for the formation of protonated methanol clusters $H^+(CH_3OH)_n$ with $n = 3-5$ to check the accuracy of our system over a wide temperature range and to provide confidence in the measured binding energy of the benzene dimer cation.

Despite the similarity of the collision cross sections of benzene and fulvene cations in a helium buffer gas, the two ions can be readily separated in the presence of the benzene neutral in the drift cell. This suggests that isomer ions with similar mobilities can be separated on the basis of the degree of their associations with the neutral precursor in the drift cell. This novel concept of the separation of isomeric ions by dimer formation is expected to be of general application and may help to resolve important outstanding issues in the separation, structure, and chemistry of hydrocarbon radical cations. Future studies will address these points.

The binding energy of a mass-selected and isomer-specific benzene cation with neutral benzene has been measured as 17.6 ± 1 and 17.4 ± 1 kcal/mol for the $(C_6H_6)_2^{+\bullet}$ and $(C_6D_6)_2^{+\bullet}$ systems, respectively. These values are similar to the value reported by Meot-Ner et al.[11] and are smaller that the more recent value reported by Hiraoka and co-workers,[17] both using pulsed high-pressure mass spectrometry.

The binding energies of the proton-bound dimers in the pyridine and triethylamine systems have been measured as 25.2 ± 1 and 20.9 ± 1 kcal/mol, respectively. A comparison of the binding energies of the benzene dimer cation and the protonated pyridine dimer indicates that the relative magnitude of charge-resonance stabilization in the benzene dimer cation is comparable to half the strength of a typical ionic hydrogen-bonding interaction. The binding energies of the protonated methanol clusters $H^+(CH_3OH)_n$ with $n = 3-5$ have been measured as 21.0, 14.3, and 11.3 kcal/mol, respectively. The excellent agreement of all of the measured binding energies with literature data establish the validity of using our new drift cell instrument to measure the thermochemical properties of association reactions involving molecular cations and protonated molecules. The combination of thermochemical properties with the structural information obtained by measuring the collision cross sections of the association product ions provides a unique opportunity to investigate the structure−property relationship in these systems.

Acknowledgment. It is a pleasure to acknowledge invaluable discussions with Drs. M. T. Bowers, M. F. Jarrold, D. E. Clemmer and P. R. Kemper regarding the ion mobility technique. The authors gratefully acknowledge financial support from the National Science Foundation (CHE- 9816536).

References and Notes

(1) Stone, A. J. *The Theory of Intermolecular Forces*; Clarendon Press: Oxford, U.K., 1996.

(2) Israelachvili, J. N. *Intermolecular and Surface Forces*; Academic Press: London, 1997.

(3) Burley, S. K.; Petsko, G. A. *Science* **1985**, *229*, 23.

(4) Smithrud, D. B.; Diederich, F. *J. Am. Chem. Soc*. **1990**, *112*, 339.

(5) Hunter, C. A.; Sanders, J. K. M. *J. Am. Chem. Soc*. **1990**, *112*, 5525.

(6) Hobza, P.; Selzle, H. L.; Schlag, E. W. *Chem. Rev*. **1994**, *94*, 1767.

(7) Rebek, J., Jr. *Chem. Soc. Rev*. **1996**, *25*, 255.

(8) Fyfe, M. C. T.; Stoddart, J. F. *Acc. Chem. Res*. **1997**, *10*, 3393.

(9) Badger, B.; Brocklehurst, B. *Nature* **1968**, *219*, 263.

(10) Field, F. H.; Hamlet, P.; Libby, W. F. *J. Am. Chem. Soc*. **1969**, *91*, 2839.

(11) Meot-Ner (Mautner), M.; Hamlet, P.; Hunter, E. P.; Field, F. H. *J. Am. Chem. Soc*. **1978**, *100*, 5466.

(12) Chandra, A. K.; Bhanuprakash, K.; Jyoti Bhasu, V. C.; Srikanthan, D. *Mol. Phys*. **1984**, *52*, 733.

(13) Liu, S.; Jarrold, M. F.; Bowers, M. T. *J. Phys. Chem*. **1985**, *89*, 3127.

(14) Grover, J. R.; Walters, E. A.; Hui, E. T. *J. Phys. Chem*. **1987**, *91*, 3233.

(15) Snodgrass, T. T.; Dunbar, R. C.; Bowers, M. T. *J. Phys. Chem*. **1990**, *94*, 3648.

(16) Ohashi, K.; Nishi, N. *J. Chem. Phys*. **1991**, *95*, 4002.

(17) Hiraoka, K.; Fujimaki, S.; Aruga, K. *J. Chem. Phys*. **1991**, *95*, 8413.

(18) Beck, S. M.; Hecht, J. H. *J. Chem. Phys*. **1992**, *96*, 1975.

(19) Bornsen, K. O.; Selzle, H. L.; Schlag, E. W. *Chem. Phys. Lett*. **1992**, *190*, 497.

(20) Meot-Ner (Mautner), M. M.; Lias, S. G.; Binding Energies Between Ions and Molecules and The Thermochemistry of Cluster Ions. In *NIST Chemistry WebBook*; Linstrom, P. J., Mallard, W. G., Eds.; NIST Standard Reference Database Number 69; National Institute of Standards and Technology: Gaithersburg, MD, July 2001 (http://webbook.nist.gov).

(21) von Helden, G.; Hsu, M. T.; Gotts, N. G.; Bowers, M. T. *J. Phys. Chem*. **1993**, *97*, 8182.

(22) von Helden, G.; Kemper, P. R.; Gotts, N. G.; Bowers, M. T. *Science* **1993**, *259*, 1300.

(23) Bowers, M. T. *Acc. Chem. Res*. **1994**, *27*, 324.

(24) Jarrold, M. F. *J. Phys. Chem*. **1995**, *99*, 11.

(25) Mesleh, M. F.; Hunter, J. M.; Shvartsburg, A. A.; Schatz, G. C.; Jarrold, M. F. *J. Phys. Chem*. **1996**, *100*, 16082.

(26) Gidden, J.; Wyttenbach, T.; Jackson. A. T.; Scrivens, J. H.; Bowers, M. T. *J. Am. Chem. Soc*. **2000**, *122*, 4692.

(27) Clemmer, D. E.; Jarrold, M. F. *J. Mass Spectrom*. **1997**, *32*, 577.

(28) El-Shall, M. S.; Marks, C.; Sieck, L. W.; Meot-Ner (Mautner), M. *J. Phys. Chem*. **1996**, *96*, 2045.

(29) Meot-Ner (Mautner), M. *J. Am. Chem. Soc*. **1986**, *108*, 6189.

(30) Grimsrud, E. P.; Kebarle, P. *J. Am. Chem. Soc*. **1973**, *95*, 7939.

(31) Rusyniak, M.; Ibrahim, Y.; Wright, D.; Khanna, S.; El-Shall, M. S. *J. Am. Chem. Soc*., submitted for publication, 2003.

(32) McDaniel, E. W.; Mason, E. A. *The Mobility and Diffusion of Ions in Gases*; Wiley & Sons: New York, 1973.

(33) Center-of-mass energy (E_{CM}) is calculated as $E_{CM} = (E_{lab}m)/(m + M)$, where m and M are the masses of the neutral and ion, respectively. See Armentrout, P. B. *J. Am. Mass Spectrom*. **2002**, *13*, 419.

(34) Rosenstock, H. M.; Larkins, J. T.; Walker, J. A. *Int. J. Mass Spectrom. Ion Phys*. **1973**, *11*, 309.

(35) Rosenstock, H. M.; Dannacher, J.; Liebman, J. F. *Radiat. Phys. Chem*. **1982**, *20*, 7.

(36) Jarrold, M. F.; Wagner-Redeker, W.; Illies, A. J.; Kirchner. N. J.; Bowers, M. T. *Int. J. Mass Spectrom. Ion Processes* **1984**, *58*, 63.

(37) Kuhlewind, H.; Kiermeier, Neusser, H. J. *J. Chem. Phys*. **1986**, *85*, 4427.

(38) van der Hart, W. J.; de Koning, L. J.; Nibbering, N. M. M.; Gross, M. L. *Int. J. Mass Spectrom. Ion Processes* **1986**, *72*, 99.

(39) Lifshitz, C.; Ohmichi, N. *J. Phys. Chem*. **1986**, *93*, 6329.

(40) Klippenstein, S. J.; Faulk, J. D.; Dunbar, R. C. *J. Chem. Phys* **1993**, *98*, 243.

(41) van de Guchte, W. J.; van der Hart, W. J.; de Koning, L. J.; Nibbering, N. M. M.; Dunbar, R. C. *Int. J. Mass. Spectrom. Ion Processes* **1993**, *123*, 11.

(42) van der Hart, W. J. *Int. J. Mass. Spectrom. Ion Processes* **1994**, *130*, 173.

(43) Chawala, R.; Shukla, A.; Futrell, J. *Int. J. Mass. Spectrom. Ion Processes* **1997**, *165/166*, 237.

(44) Gross, M. L.; Russell, D. H.; Aerni, R. J.; Bronczyk, S. A., *J. Am. Chem. Soc*. **1977**, *99*, 3603.

(45) Russell, D. H.; Gross, M. L. *J. Am. Chem. Soc*. **1980**, *102*, 6279.

(46) Miller, D. L.; Gross, M. L. *J. Am. Chem. So*c. **1983**, *105*, 3783.

(47) *NIST Chemistry WebBook*; Linstrom, P. J., Mallard, W. G., Eds.; NIST Standard Reference Database Number 69; National Institute of Standards and Technology: Gaithersburg MD, July 2001 (http://webbook.nist.gov).

(48) Viehland, L. A.; Mason, E. A. *At. Data Nucl. Data Tables* **1995**, *60*, 37−95.

(49) Ellis, H. W.; McDaniel, E. W.; Albritton, D. L.; Viehland, L. A.; Lin, S. L.; Mason, E. A. *At. Data Nucl. Data Tables* **1978**, *22*, 179−217.

(50) Krishnamurthy, M.; de Gouw, J. A.; Bierbaum, V. M.; Leone, S. R. *J. Phys. Chem*. **1996**, *100*, 14908.

(51) Mason, E. A.; McDaniel, E. W. *Transport Properties of Ions in Gases*, Wiley & Sons: New York, 1988.

(52) Revercomb, H. W.; Mason, E. A. *Anal. Chem*. **1975**, *47*, 970.

(53) Hirschfelder, J. O.; Curtiss, C. F.; Bird, R. B. *Molecular Theory of Gases and Liquids*; Wiley: New York, 1954.

(54) The ab initio calculations were carried out using Gaussian 98: Frisch, M. J.; Trucks, G. W.; Schlegel, H. B.; Scuseria, G. E.; Robb, M. A.; Cheeseman, J. R.; Zakrzewski, V. G.; Montgomery, J. A., Jr.; Stratmann, R. E.; Burant, J. C.; Dapprich, S.; Millam, J. M.; Daniels, A. D.; Kudin, K. N.; Strain, M. C.; Farkas, O.; Tomasi, J.; Barone, V.; Cossi, M.; Cammi, R.; Mennucci, B.; Pomelli, C.; Adamo, C.; Clifford, S.; Ochterski, J.; Petersson, G. A.; Ayala, P. Y.; Cui, Q.; Morokuma, K.; Malick, D. K.; Rabuck, A. D.; Raghavachari, K.; Foresman, J. B.; Cioslowski, J.; Ortiz, J. V.; Stefanov, B. B.; Liu, G.; Liashenko, A.; Piskorz, P.; Komaromi, I.; Gomperts, R.; Martin, R. L.; Fox, D. J.; Keith, T.; Al-Laham, M. A.; Peng, C. Y.; Nanayakkara, A.; Gonzalez, C.; Challacombe, M.; Gill, P. M. W.; Johnson, B. G.; Chen, W.; Wong, M. W.; Andres, J. L.; Head-Gordon, M.; Replogle, E. S.; Pople, J. A. *Gaussian 98*, revision A.11.3; Gaussian, Inc.: Pittsburgh, PA, 2002.

(55) Beynon, J. H.; Caprioli, R. M.; Perry, W. O.; Baitinger, W. E. *J. Am. Chem. Soc*. **1972**, *94*, 6828.

(56) Gross, M. L.; Aerni, R. J. *J. Am. Chem. Soc*. **1973**, *95*, 7875.

(57) Neuhauser, R. G.; Siglow, K.; Neusser, H. J. *J. Chem. Phys*. **1997**, *106*, 896.

(58) Inokuchi, Y.; Ohashi, K.; Nishi, N. *Chem. Phys. Lett*. **1997**, *279*, 73.

(59) Meot-Net (Mautner), M. *J. Am. Chem. Soc*. **1992**, *114*, 3312.

(60) Meot-Ner (Mautner), M.; Sieck, L. W. *J. Am. Chem. Soc*. **1983**, *105*, 2956.

(61) Meot-Net (Mautner), M. *J. Am. Chem. Soc*. **1979**, *101*, 2396.

(62) Holland, P. M.; Castleman, A. W. *J. Chem. Phys*. **1982**, *76*, 4195.

(63) Meot-Net (Mautner), M. *J. Phys. Chem*. **1980**, *84*, 2724.

(64) El-Shall, M. S.; Meot-Net (Mautner), M. *J. Phys. Chem*. **1987**, *91*, 1088.